AIAA 2007-3479

CrossMark
click for updates

13th AIAA/CEAS Aeroacoustics Conference, May 21—23, Rome, Italy

A Three-dimensional Time-domain Boundary Element Method for the Computation of Exact Green's Functions in Acoustic Analogy

Andrea D. Jones*, Fang Q. Hu†

*†Old Dominion University, Norfolk, Virginia 23529, USA

A three-dimensional time-domain Boundary Element Method is formulated for solving exact Green's functions numerically. The use of triangular boundary elements and interior collocation points allows application of the method to complex boundaries. A March-On-Time scheme is used to determine exact Green's functions at several frequencies in a single calculation. Long-time stability is accomplished via a modified Burton-Miller boundary integral equation. A Fast Fourier Transform of the time-dependent numerical solution is used to compare numerical results with the exact solution for a sphere in the frequency domain. The effects of changing two boundary integral equation parameters and the time step size are discussed. By decreasing the time step size, the numerical solution becomes more accurate until a minimum value that depends on the frequency is reached. With proper parameter choices and time step size, the modified Burton-Miller time-domain Boundary Element Method produces accurate and stable numerical results.

Downloaded by Fang Hu on August 28, 2016 | http://arc.aiaa.org | DOI: 10.2514/6.2007-3479

I. Introduction

A Green's function that satisfies all the boundary conditions is often referred to as the exact or the tailored Green's function. It is well known in the theory of acoustic analogy that when an exact Green's function is used, the far field sound can be expressed as a volume integral involving the Lighthill tensors and the double divergence of the Green's function. The use of the exact Green's function allows the development of noise prediction strategy based on steady flow simulations with direct noise source modelings.[1] The computation of the exact Green's function, as well as its double divergence, becomes an integral part of this noise prediction strategy.

In earlier studies, a spectral collocation boundary element method for solving the convective wave equation in the frequency domain with a constant mean flow was developed for arbitrary two-dimensional bodies.[2,3] In this paper, we present a time-domain Boundary Element Method for the computation of exact Green's functions for general three-dimensional surfaces. The extension of exact Green's function computation to three-dimensional geometries is by no means trivial. The main challenge is achieving the computational efficiency necessary for routine use of the exact Green's function as a practical tool. This involves overcoming the computational difficulty that results from the extremely large degrees of freedom at mid to high frequencies of typical airframe acoustic radiation when the body of the entire aircraft, or a large component of which, is included. The time-domain approach has several advantages. First, the inversion of a large, dense matrix is not required. Next, exact Green's functions at all frequencies are contained in a single computation. Finally, the computational complexity can be reduced to $O(N_t N \log^2 N)$ where N_t is the number of time steps and N is the total number of spatial basis functions, making the method feasible for routine application at mid to high frequencies.[4,5]

The time-domain boundary integral equation will be solved using a spectral collocation method on triangular boundary elements. The use of triangular elements makes our method flexible and easily applicable

*Graduate student, Department of Mathematics and Statistics, student member AIAA
†Professor, Department of Mathematics and Statistics, Senior member AIAA

Copyright © 2007 by Andrea Jones and Fang Hu. Published by the American Institute of Aeronautics and Astronautics, Inc., with permission.

to complex bodies. The spectral node distribution over the triangle in the parametric plane is chosen to be the interior points proposed by Strang and Fix.[6] The corresponding spatial basis functions are linear combinations of the Proriol orthogonal polynomials.[7] A March-On-Time (MOT) is developed in which third order basis functions are used for approximating the time dependency. Long-time stability is achieved using a modified Burton-Miller boundary integral equation. The temporal point source is modeled by a finite transient signal and the exact Green's functions at all frequencies are obtained in a single calculation through the Fast Fourier Transform (FFT) of the time-dependent numerical solution.

The rest of the paper is organized as follows. In section II, the three-dimensional time-domain Boundary Element Method used in this investigation is formulated via a March-On-Time approach. The discretization of the boundary into triangular elements and the choice of spatial and temporal basis functions are discussed. Numerical solutions are presented in section III for the case of a spherical boundary. In section IV, long-time solution instabilities resulting from the March-On-Time scheme are eliminated using a modified Burton-Miller Combined Field Integral Equation. The treatment of hypersingular integrals that arise when applying the modified Burton-Miller scheme is also discussed in section IV. Section V contains numerical results for a spherical boundary using the modified Burton-Miller Boundary Integral Equation. The effects of changing two parameters in the boundary integral equation along with the effect of changing the time step size are discussed. Section VI contains the conclusions.

II. Formulation of the Time-domain Boundary Element Method

II.A. The March-On-Time Method

An exact Green's function, $g(\mathbf{x},\mathbf{y},t,s)$, is defined as the solution to the convective wave equation

$$(\frac{\partial}{\partial t}+\mathbf{U}\cdot\nabla)^2 g(\mathbf{x},\mathbf{y},t,s)-\nabla^2 g(\mathbf{x},\mathbf{y},t,s)=\delta(t-s)\delta(\mathbf{x}-\mathbf{y}) \tag{1}$$

with boundary condition

$$\mathbf{n}\cdot\nabla g=0 \tag{2}$$

on all solid surfaces where $\mathbf{n}$ is the normal vector out of the fluid. By using a free-space Green's function, the convective wave equation (1), together with the boundary condition (2), can be cast into a boundary integral equation as

$$4\pi C_s g(\mathbf{z}_s,\mathbf{y},t,s)=\frac{q(t-s-|\mathbf{y}-\mathbf{z}_s|)}{|\mathbf{y}-\mathbf{z}_s|}+\int_S\Big[\frac{1}{R^2}[\frac{\partial R}{\partial n}-U_{\mathbf{n}}(\mathbf{U}\cdot\nabla R)]g(\mathbf{x}_s,\mathbf{y},t_{_R},s)$$

$$+\frac{1}{R}[\frac{\partial R}{\partial n}-2U_{\mathbf{n}}-U_{\mathbf{n}}(\mathbf{U}\cdot\nabla R)]\frac{\partial g}{\partial t}(\mathbf{x}_s,\mathbf{y},t_{_R},s)-\frac{U_{\mathbf{n}}}{R}[\mathbf{U}\cdot\nabla g(\mathbf{x}_s,\mathbf{y},t_{_R},s)]\Big]d\mathbf{x}_s \tag{3}$$

where $R=|\mathbf{x}_s-\mathbf{z}_s|$, $\mathbf{z}_s$ is a point on the body surface S, and $\mathbf{x}_s$ is the surface integration variable. In equation (3), C_s is a constant and $t_{_R}=t-R$. For computational purposes, the time delta function $\delta(t-s)$ has been replaced by a finite continuous function $q(t-s)$ which has a spectrum of unity over the range of frequency of interest. Consider the Fourier transform in time

$$\widehat{q}\,(\omega)=\frac{1}{2\pi}\int_{-\infty}^{\infty}q(t)e^{i\omega t}dt$$

with inverse

$$q(t)=\int_{-\infty}^{\infty}\widehat{q}\,(\omega)\,e^{-i\omega t}d\omega$$

Let

$$\widehat{q}\,(\omega)=\begin{cases}1 & |\omega|\le\omega_0\\ 0.5+0.5\cos\left(\frac{\omega-\omega_0}{2h}\pi\right) & \omega_0\le\omega\le\omega_0+2h\\ 0.5+0.5\cos\left(\frac{\omega+\omega_0}{2h}\pi\right) & -\omega_0-2h\le\omega\le-\omega_0\end{cases}$$

where ω_0 is the source function frequency and h is a parameter that determines the shape of q. Then,

$$q(t)=\frac{2\pi^2}{t\,(\pi^2-4h^2t^2)}\sin\left(\omega_0 t+ht\right)\cos(ht)$$

Downloaded by Fang Hu on August 28, 2016 | http://arc.aiaa.org | DOI: 10.2514/6.2007-3479

The boundary integral equation (3) represents a reduction in spatial dimensions from 3D to 2D and hence, only a surface mesh is required for discretization instead of a volume mesh. Aside from the obvious benefit of increased computational efficiency, the Boundary Element Method has low storage requirements compared to 3D volume based methods and the far-field radiation condition is automatically satisfied. Once $g(\mathbf{x}, \mathbf{y}, t, s)$ is found, the frequency domain solution $\tilde{g}(\mathbf{x}, \mathbf{y}, \omega, s)$ for use in the acoustic analogy formula can be obtained by a Fourier transform in time, for any given frequency ω such that $|\omega| \leq \omega_0 + 2h$.

To solve the boundary integral equation (3), we expand the solution on the surface of the body as

$$g(\mathbf{x}_s, \mathbf{y}, t, s) = \sum_{n=0}^{N_t} \sum_{i=1}^{N} u_i^n \phi_i(\mathbf{x}_s) \psi_n(t) \tag{4}$$

where $\{\phi_i(\mathbf{x}_s)\}$ is a set of basis functions covering the surface of the body and $\{\psi_n(t)\}$ is the set of basis functions for time t. By substituting (4) into the integral equation (3), a linear system of equations is obtained for the expansion coefficients u_i^n. The advantage here is that this system can be solved by a March-On-Time (MOT) method, which does not require the inversion of a large dense matrix as in the frequency domain formulation. Consider equation (3) in the absence of mean flow,

$$4\pi C_s g(\mathbf{z}_s, \mathbf{y}, t, s) = \frac{1}{r} q(t - s - r) + \int_S \frac{1}{R^2} \frac{\partial R}{\partial n} [g]_{t_R} d\mathbf{x}_s + \int_S \frac{1}{R} \frac{\partial R}{\partial n} \left[\frac{\partial g}{\partial t} \right]_{t_R} d\mathbf{x}_s \tag{5}$$

where $R = |\mathbf{x}_s - \mathbf{z}_s|$, $r = |\mathbf{y} - \mathbf{z}_s|$. By substituting (4) into (5), and forcing the equation to be satisfied at collocation point $\mathbf{z}_s = \mathbf{x}_k$ and time level t_j, we get

$$4\pi C_s \sum_{n=0}^{N_t} \sum_{i=1}^{N} u_i^n \phi_i(\mathbf{x}_k) \psi_n(t_j) = \frac{1}{r} q(t_j - s - r) + \int_S \frac{1}{R^2} \frac{\partial R}{\partial n} \sum_{n=0}^{N_t} \sum_{i=1}^{N} u_i^n \phi_i(\mathbf{x}_s) \psi_n(t_j - R) d\mathbf{x}_s$$

$$+ \int_S \frac{1}{R} \frac{\partial R}{\partial n} \sum_{n=0}^{N_t} \sum_{i=1}^{N} u_i^n \phi_i(\mathbf{x}_s) \psi_n'(t_j - R) d\mathbf{x}_s$$

for $k = 1, 2, ..., N$ and $j = 1, 2, ..., N_t$. By the property of causality,

$$\psi_n(t_j) \equiv 0 \quad \text{for } j > n$$

the above can be written as a time marching scheme as

$$\mathbf{B}_0 \mathbf{u}^j = \mathbf{q}^j - \sum_{m=1}^{j} \mathbf{B}_m \mathbf{u}^{j-m} \tag{6}$$

where $\mathbf{u}^j$ represents the vector containing all unknowns at time level t_j, $\mathbf{u}^j = \begin{bmatrix} u_1^j & u_2^j & \cdot & \cdot & \cdot & u_N^j \end{bmatrix}$. Equation (6) relates the solution at the current time level $t = t_j$ to the solutions at all previous time levels. Specifically, at time level t_j, the rows and columns of matrix $\mathbf{B}_m$ are

$$\{\mathbf{B}_m\}_{ki} = -\int_S \frac{1}{R^2} \frac{\partial R}{\partial n} \phi_i(\mathbf{x}_s) \psi_{j-m}(t_j - R) d\mathbf{x}_s - \int_S \frac{1}{R} \frac{\partial R}{\partial n} \phi_i(\mathbf{x}_s) \psi_{j-m}'(t_j - R) d\mathbf{x}_s$$

$$+ 4\pi C_s \phi_i(\mathbf{x}_k) \psi_{j-m}(t_j) \tag{7}$$

where $R = |\mathbf{x}_s - \mathbf{x}_k|$ and $\mathbf{B}_0$ is formed from $\mathbf{B}_m$ when $m = 0$. At each time level, t_j, the matrix $\mathbf{B}_0$ is a sparse matrix, which can be solved using iterative methods in order to improve computational efficiency.

II.B. Triangular Boundary Elements

An open or closed three-dimensional surface can be divided into flat or curved triangles.[8] Triangular boundary elements are more robust when dealing with arbitrary geometries than quadrilateral elements. Let the body surface, S, be discretized into a grid of curved or flat triangular elements, E_α. Each element is mapped to a flat right isosceles element, D, in the parametric ξ, η-plane as shown in Figure 1.[9] The spectral node distribution over the triangle in the parametric plane is chosen to be the interior points proposed by Strang and Fix.[6] Interior collocation points are used so that the scheme can be applied to any geometry. An inverse mapping from D onto each element E_α determines the location of each node i on the body surface, S.

Downloaded by Fang Hu on August 28, 2016 | http://arc.aiaa.org | DOI: 10.2514/6.2007-3479

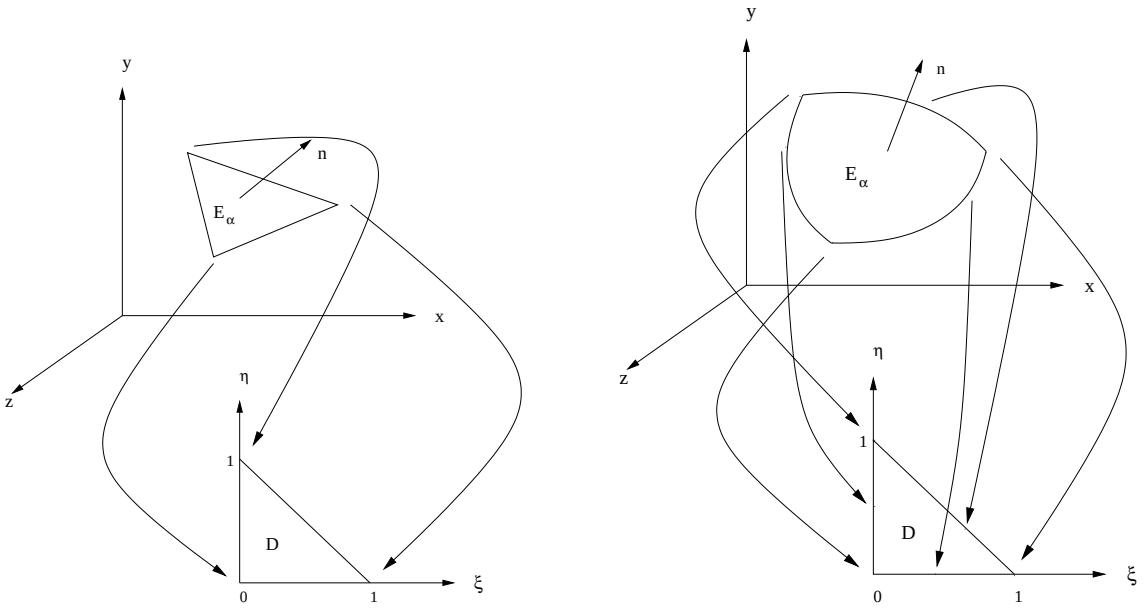

Figure 1. A three-node (left) and a six-node (right) triangle in three-dimensional space mapped to a right isosceles triangle in the parametric plane.

Downloaded by Fang Hu on August 28, 2016 | http://arc.aiaa.org | DOI: 10.2514/6.2007-3479

II.C. Discussion of Basis Functions

II.C.1. Temporal Basis Functions

The temporal basis functions chosen for the time-domain Boundary Element Method are cubic interpolation functions defined as

$$\psi_j(t) = \Psi(t - t_j)$$

where $t_j = j\Delta t$. The basis functions are defined as

$$\Psi(t) = \begin{cases} 1 + \frac{11}{6}(\frac{t}{\Delta t}) + (\frac{t}{\Delta t})^2 + \frac{1}{6}(\frac{t}{\Delta t})^3 & \text{for } -\Delta t \le t \le 0 \\ 1 + \frac{1}{2}(\frac{t}{\Delta t}) - (\frac{t}{\Delta t})^2 - \frac{1}{2}(\frac{t}{\Delta t})^3 & \text{for } 0 < t \le \Delta t \\ 1 - \frac{1}{2}(\frac{t}{\Delta t}) - (\frac{t}{\Delta t})^2 + \frac{1}{2}(\frac{t}{\Delta t})^3 & \text{for } \Delta t < t \le 2\Delta t \\ 1 - \frac{11}{6}(\frac{t}{\Delta t}) + (\frac{t}{\Delta t})^2 - \frac{1}{6}(\frac{t}{\Delta t})^3 & \text{for } 2\Delta t < t \le 3\Delta t \\ 0 & \text{elsewhere} \end{cases}$$

and the nonzero part is shown graphically in Figure 2. Then, the expression for the $\mathbf{B}$ matrices can be written as

$$\{\mathbf{B}_m\}_{ki} = -\int_S \frac{1}{R^2}\frac{\partial R}{\partial n}\phi_i(\mathbf{x}_s)\,\Psi(t_j - R - t_{j-m})\,d\mathbf{x}_s - \int_S \frac{1}{R}\frac{\partial R}{\partial n}\phi_i(\mathbf{x}_s)\,\Psi'(t_j - R - t_{j-m})\,d\mathbf{x}_s$$
$$+4\pi C_s \phi_i(\mathbf{x}_k)\,\Psi(t_j - t_{j-m})$$

or

$$\{\mathbf{B}_m\}_{ki} = -\int_S \frac{1}{R^2}\frac{\partial R}{\partial n}\phi_i(\mathbf{x}_s)\,\Psi(m\Delta t - R)\,d\mathbf{x}_s - \int_S \frac{1}{R}\frac{\partial R}{\partial n}\phi_i(\mathbf{x}_s)\,\Psi'(m\Delta t - R)\,d\mathbf{x}_s$$
$$+4\pi C_s \phi_i(\mathbf{x}_k)\,\Psi(m\Delta t) \tag{8}$$

In equation (8), the $\mathbf{B}$ matrices are independent of time t. As a result, each $\mathbf{B}$ matrix is computed only once and stored in computer memory for future use.

Furthermore, by the definition of the temporal basis functions, $\Psi(m\Delta t - R) = 0$ when

$$m\Delta t - R > 3\Delta t$$

or

$$m > \frac{R + 3\Delta t}{\Delta t}$$

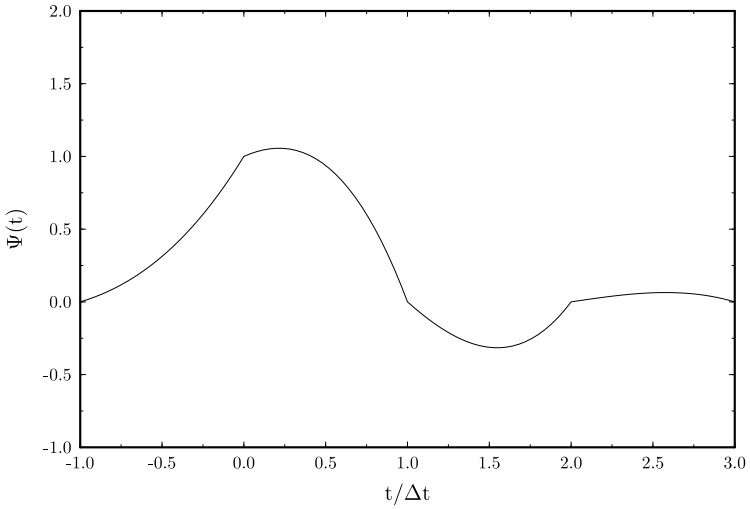

Figure 2. Temporal Basis Function $\Psi(t)$.

Downloaded by Fang Hu on August 28, 2016 | http://arc.aiaa.org | DOI: 10.2514/6.2007-3479

This implies that all entries of a $\mathbf{B}_m$ matrix are zero when

$$m > \frac{R_{\max}}{\Delta t} + 3$$

where $R_{\max}$ is the maximum dimension of the three-dimensional body. For the case when $m = 0$, the matrix $\mathbf{B}_0$ is given as

$$\{\mathbf{B}_0\}_{ki} = -\int_S \frac{1}{R^2}\frac{\partial R}{\partial n}\phi_i\left(\mathbf{x}_s\right)\Psi\left(-R\right)d\mathbf{x}_s - \int_S \frac{1}{R}\frac{\partial R}{\partial n}\phi_i\left(\mathbf{x}_s\right)\Psi'\left(-R\right)d\mathbf{x}_s$$
$$+4\pi C_s\phi_i\left(\mathbf{x}_k\right)\Psi(0) \tag{9}$$

If the time step is chosen such that

$$\Delta t < R_{min}$$

then

$$\Psi(-R) = 0$$

except when $R = 0$, i.e., $k = i$. Consequently, $\mathbf{B}_0$ will be a diagonal matrix when Δt is chosen to be less than the minimum distance between collocation point and quadrature points.

II.C.2. Spatial Basis Functions

The spatial basis function for node i, $\phi_i(\mathbf{x}_s)$, satisfies

$$\phi_i(\mathbf{x}_k) = \begin{cases} 1 & k = i \\ 0 & k \neq i \end{cases}$$

for $k = 1, ..., N$ and $i = 1, ..., N$ where N is the total number of spatial basis functions. Hence, $\phi_i(\mathbf{x}_s)$ is non-zero only on one element since i is an interior node. Let the quadrature formula for the surface integrals in the $\mathbf{B}$ matrices be

$$\int_{E_\alpha} F(\mathbf{x}_s)d\mathbf{x}_s = \sum_{\beta=1}^{N_p} w_\beta F(\mathbf{x}_\beta^\alpha)$$

where $\mathbf{x}_\beta^\alpha$ and w_β are the quadrature points and weights on element E_α. Then, the integrals in the $\mathbf{B}_m$ matrices have the form

$$\int_S \frac{1}{R^2}\frac{\partial R}{\partial n}\phi_i(\mathbf{x}_s)\Psi(m\Delta t - R)d\mathbf{x}_s = \sum_\alpha \int_{E_\alpha} \frac{1}{R^2}\frac{\partial R}{\partial n}\phi_i(\mathbf{x}_s)\Psi(m\Delta t - R)d\mathbf{x}_s$$

$$= \sum_{\alpha} \sum_{\beta} w_\beta \frac{1}{R^2} \frac{\partial R}{\partial n} \phi_i(\mathbf{x}_\beta^\alpha) \Psi(m\Delta t - R) J_\alpha \tag{10}$$

where $R = |\mathbf{x}_\beta^\alpha - \mathbf{x}_k|$. In equation (10), E_α is the element that supports node i and β is the quadrature point index for the element after it has been mapped to the base right triangle, i.e., domain D. Also, J_α is the Jacobian for element E_α when it is mapped to the base right triangle.

The basis function for each node corresponds to a linear combination of a set of independent polynomials in the parametric plane defined as

$$\phi_i(\mathbf{x}_s) = \sum_{\ell=1}^{P} c_\ell^j T_\ell(\xi, \eta) \tag{11}$$

for $j = 1, ..., P$. One suitable basis set for the functions $T_\ell(\xi, \eta)$ is the set comprised of Proriol's orthogonal polynomials.[7,9] The Proriol polynomials involve monomials of the form $\xi^p \eta^{(m-p+q)}$ with combined order $m + q$, for $p = 1, 2, ..., m$ and $q = 1, 2, ..., n$ and are given by

$$\mathsf{P}_{mn} = L_m(\xi')(1-\eta)^m J_n^{(2m+1,0)}(\eta')$$

where

$$\xi' = \frac{2\xi}{1-\eta} - 1, \qquad \eta' = 2\eta - 1,$$

L_m are Legendre polynomials and $J_n^{(2m+1,0)}$ are Jacobi polynomials.

II.D. Treatment of Kernel Singularities

Consider the first integral in equation (8), given by

$$\int_S \frac{1}{R^2} \frac{\partial R}{\partial n} \phi_i(\mathbf{x}_s) \Psi(m\Delta t - R) \, d\mathbf{x}_s$$

and note that $R = |\mathbf{x}_s - \mathbf{x}_k|$ and

$$\frac{1}{R^2} \frac{\partial R}{\partial n} = \frac{\mathbf{n}_s \cdot (\mathbf{x}_s - \mathbf{x}_k)}{|\mathbf{x}_s - \mathbf{x}_k|^3}$$

Hence, the integral kernel is singular when integration is being performed on the element containing $\mathbf{x}_k$. Let the element be parameterized as

$$\mathbf{x}(\xi, \eta) = \mathbf{a} + \mathbf{b}\xi + \mathbf{c}\eta + \mathbf{d}\xi^2 + \mathbf{e}\eta^2 + \mathbf{f}\xi\eta$$

so that

$$\mathbf{x}_k(\xi, \eta) = \mathbf{a} + \mathbf{b}\xi_k + \mathbf{c}\eta_k + \mathbf{d}\xi_k^2 + \mathbf{e}\eta_k^2 + \mathbf{f}\xi_k\eta_k$$
$$\mathbf{x}_s(\xi, \eta) = \mathbf{a} + \mathbf{b}\xi_s + \mathbf{c}\eta_s + \mathbf{d}\xi_s^2 + \mathbf{e}\eta_s^2 + \mathbf{f}\xi_s\eta_s$$

Then,

$$\int_S \frac{1}{R^2} \frac{\partial R}{\partial n} \phi_i(\mathbf{x}_s) \Psi(m\Delta t - R) d\mathbf{x}_s = \int\int_S \frac{\mathbf{n}_s \cdot (\mathbf{x}_s - \mathbf{x}_k)}{|\mathbf{x}_s - \mathbf{x}_k|^3} \phi_i(\mathbf{x}_s) \Psi(m\Delta t - |\mathbf{x}_s - \mathbf{x}_k|) \cdot |\mathbf{x}_\xi \times \mathbf{x}_\eta| \, d\xi d\eta$$

Note that

$$\mathbf{x}_s - \mathbf{x}_k = \mathbf{b}(\xi_s - \xi_k) + \mathbf{c}(\eta_s - \eta_k) + \mathbf{d}\left(\xi_s^2 - \xi_k^2\right) + \mathbf{e}\left(\eta_s^2 - \eta_k^2\right) + \mathbf{f}(\xi_s\eta_s - \xi_k\eta_k)$$

Let

$$\xi_s - \xi_k = r\cos\theta, \quad \eta_s - \eta_k = r\sin\theta$$

to get

$$\mathbf{x}_s - \mathbf{x}_k = \mathbf{b}r\cos\theta + \mathbf{c}r\sin\theta + \mathbf{d}\left((r\cos\theta + \xi_k)^2 - \xi_k^2\right) + \mathbf{e}\left((r\sin\theta + \eta_k)^2 - \eta_k^2\right)$$
$$+\mathbf{f}\left((r\cos\theta + \xi_k)(r\sin\theta + \eta_k) - \xi_k\eta_k\right)$$

Downloaded by Fang Hu on August 28, 2016 | http://arc.aiaa.org | DOI: 10.2514/6.2007-3479

$$= r\left(\mathbf{b}\cos\theta + \mathbf{c}\sin\theta\right) + \mathbf{d}\left(r^2\cos^2\theta + 2\xi_k r\cos\theta\right) + \mathbf{e}\left(r^2\sin^2\theta + 2\eta_k r\sin\theta\right)$$
$$+\mathbf{f}\left(r^2\cos\theta\sin\theta + \xi_k r\sin\theta + \eta_k r\cos\theta\right)$$
$$= O(r)$$

With the above change of variables, $\mathbf{n}_s$ becomes

$$\mathbf{n}_s = \frac{\mathbf{x}_\xi \times \mathbf{x}_\eta}{|\mathbf{x}_\xi \times \mathbf{x}_\eta|} = \frac{(\mathbf{b} + 2\mathbf{d}\xi_s + \mathbf{f}\eta_s) \times (\mathbf{c} + \mathbf{f}\xi_s + 2\mathbf{e}\eta_s)}{|(\mathbf{b} + 2\mathbf{d}\xi_s + \mathbf{f}\eta_s) \times (\mathbf{c} + \mathbf{f}\xi_s + 2\mathbf{e}\eta_s)|} \tag{12}$$

For points $\mathbf{x}_s$ on the same element as $\mathbf{x}_k$, the numerator of equation (12) can be written as

$$(\mathbf{b} + 2\mathbf{d}\xi_s + \mathbf{f}\eta_s) \times (\mathbf{c} + \mathbf{f}\xi_s + 2\mathbf{e}\eta_s) = (\mathbf{b} + 2\mathbf{d}\xi_k + 2\mathbf{d}r\cos\theta + \mathbf{f}\eta_k + \mathbf{f}r\sin\theta)$$
$$\times (\mathbf{c} + \mathbf{f}\xi_k + \mathbf{c} + \mathbf{f}r\cos\theta + 2\mathbf{e}\eta_k + 2\mathbf{e}r\sin\theta)$$

From here it can be shown that

$$(\mathbf{x}_\xi \times \mathbf{x}_\eta) \cdot (\mathbf{x}_s - \mathbf{x}_k) = O(r^2)$$

and

$$\frac{1}{R^2}\frac{\partial R}{\partial n} = \frac{\mathbf{n}_s \cdot (\mathbf{x}_s - \mathbf{x}_k)}{|\mathbf{x}_s - \mathbf{x}_k|^3} = O\left(\frac{1}{r}\right)$$

Thus, the integrand is integrable when the first integral in equation (8) is written in polar coordinates centered at (ξ_k, η_k) as

$$\int_{\theta_1}^{\theta_2}\int_0^{r(\theta)} \frac{1}{R^2}\frac{\partial R}{\partial n}\phi_i(\mathbf{x}_s)\psi_{j-m}(t_j - R)\,|\mathbf{x}_\xi \times \mathbf{x}_\eta|\,r dr d\theta$$

III. Results of Time-domain Boundary Element Method on Sphere

Consider a sphere of radius 0.5 with a boundary consisting of $N = 760$ curved triangular elements. Figure 3 shows the expansion coefficient, u_1^j, corresponding to the node located at $\mathbf{z}_s = (0.0514, 0.00814, 0.497)$ versus time obtained by the time-domain boundary element method at two source function frequencies ω_0. The source point is located at $\mathbf{y} = (0, 0, 10)$ and the mean flow Mach number is $M = 0$. The basis function order is $P = 0$, therefore, there is only one interior collocation point associated with each element. The time step size is $\Delta t = 0.05$.

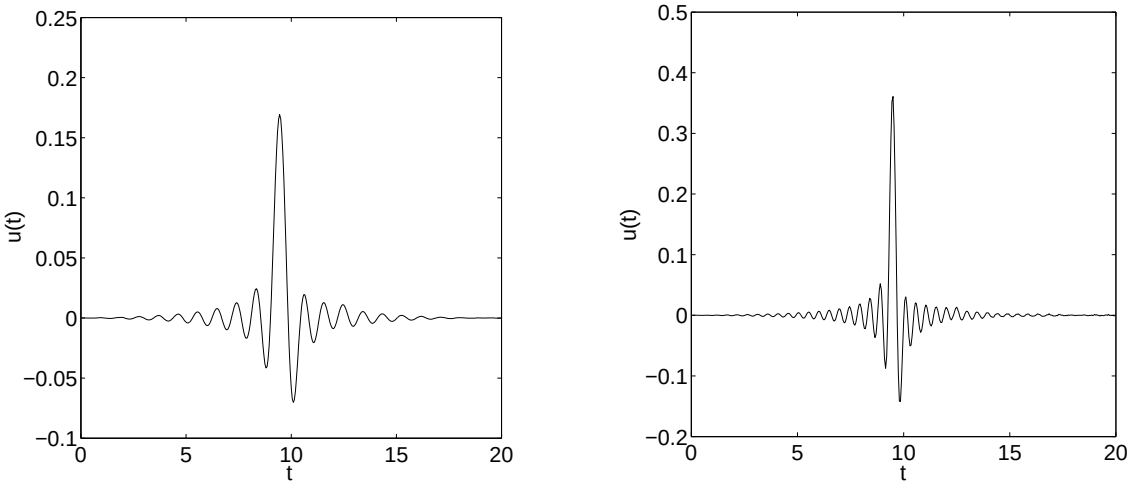

Figure 3. Transient numerical solution $u(t)$ at $\mathbf{z}_s = (0.0514, 0.00814, 0.497)$. The source function frequency is $\omega_0 = 2\pi$ (left) and $\omega_0 = 4\pi$ (right).

Unfortunately, one well-known drawback of March-On-Time schemes is the tendency towards long-time instability.[4,10] For example, consider again the sphere of radius 0.5 as described above. Figure 4 illustrates the instability caused by the MOT scheme when $\omega_0 = 6\pi$. Long-time instabilities will eventually occur for all

Downloaded by Fang Hu on August 28, 2016 | http://arc.aiaa.org | DOI: 10.2514/6.2007-3479

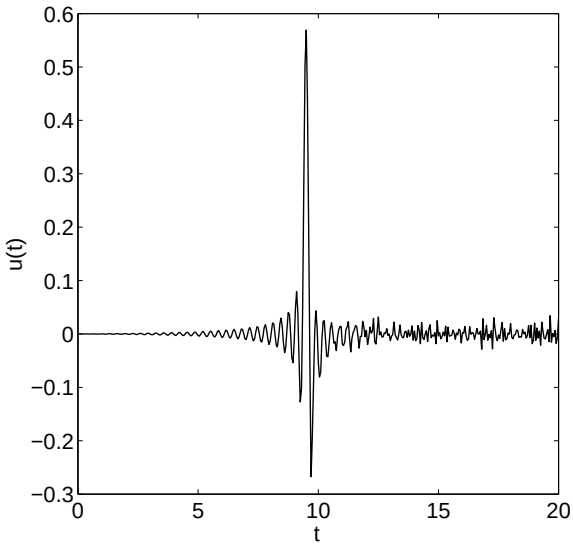

Figure 4. Transient numerical solution $u(t)$ at $\mathbf{z}_s = (0.0514, 0.00814, 0.497)$. The source function frequency is $\omega_0 = 6\pi$.

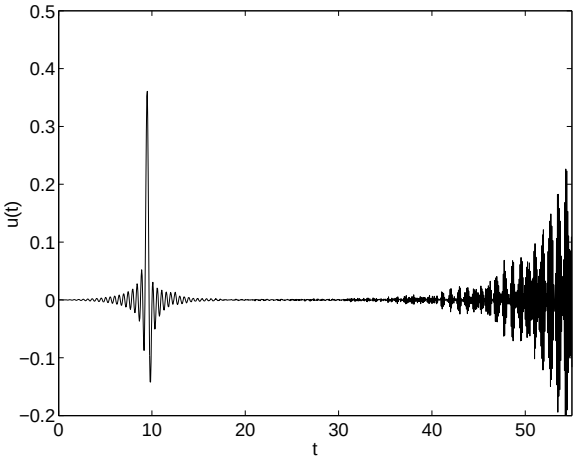

Figure 5. Transient numerical solution $u(t)$ at $\mathbf{z}_s = (0.0514, 0.00814, 0.497)$. The source function frequency is $\omega_0 = 4\pi$.

Downloaded by Fang Hu on August 28, 2016 | http://arc.aiaa.org | DOI: 10.2514/6.2007-3479

source function frequencies at varying times. Figure 5 shows the instability beginning at approximately $t = 30$ when $\omega_0 = 4\pi$. It is common knowledge that the frequency-domain solutions to Helmholtz integral equations are not unique at certain resonance frequencies. The corresponding time-domain solutions are unique by the presence of initial conditions, but due to discretization inaccuracies, resonant modes of the scatter become excited causing these solutions to contain oscillations as time marches on.[4] The loss in accuracy is more severe for higher frequencies.[10] Several methods are available to overcome long-time instabilities in time-marching numerical solutions. Some examples are time-averaging, modified time stepping, implicit MOT schemes and Galerkin approaches. The method utilized in this paper is based on Burton and Miller's formulation.[11]

IV. Burton-Miller Formulation

One of the most successful and robust approaches for overcoming the non-uniqueness problem of the frequency-domain boundary element method was introduced by Burton and Miller in 1971.[11] Their method produces a Combined Field Integral Equation (CFIE) made up of the Helmholtz integral equation and its normal derivative. The linear combination of the two equations ensures a unique solution at all frequencies.[11,12] In this section, an extension of the Burton-Miller formulation is derived following the recent analysis in [4] and [10] for the exact Green's function solution in the time-domain.

IV.A. March-On-Time Formulation

Consider the boundary integral equation derived previously, given by

$$4\pi C_s g(\mathbf{z}_s, \mathbf{y}, t, s) = \frac{q(t-s-r)}{r} + \int_S \frac{1}{R^2}\frac{\partial R}{\partial n}\left[g\right]_{t_R} d\mathbf{x}_s + \int_S \frac{1}{R}\frac{\partial R}{\partial n}\left[\frac{\partial g}{\partial t}\right]_{t_R} d\mathbf{x}_s$$

Since

$$\frac{1}{R^2}\frac{\partial R}{\partial n}\left[g\right]_{t_R} + \frac{1}{R}\frac{\partial R}{\partial n}\left[\frac{\partial g}{\partial t}\right]_{t_R} = -\frac{\partial}{\partial n}\left[\frac{1}{R}\left[g\right]_{t_R}\right]$$

the integral equation can be re-written as

$$4\pi C_s g\left(\mathbf{z}_s, \mathbf{y}, t, s\right) = \frac{1}{r} q\left(t-s-r\right) - \int_S \frac{\partial}{\partial n}\left[\frac{1}{R}\left[g\right]_{t_R}\right] d\mathbf{x}_s \tag{13}$$

Consider the integral relation obtained by a time derivative of equation (13),

$$4\pi C_s \frac{\partial g}{\partial t}\left(\mathbf{z}_s, \mathbf{y}, t, s\right) = \frac{1}{r}\frac{\partial q}{\partial t}\left(t-s-r\right) - \int_S \frac{\partial}{\partial n}\left[\frac{1}{R}\left[\frac{\partial g}{\partial t}\right]_{t_R}\right] d\mathbf{x}_s \tag{14}$$

where $R = |\mathbf{x}_s - \mathbf{z}_s|$ and $r = |\mathbf{y} - \mathbf{z}_s|$. The Burton-Miller time-domain CFIE is a linear combination of equation (14) and the normal gradient at the boundary of equation (13), given by[13]

$$4\pi \frac{\partial}{\partial n_z}[C_s g\left(\mathbf{z}_s, \mathbf{y}, t, s\right)] = \frac{\partial}{\partial n_z}\left[\frac{1}{r} q\left(t-s-r\right)\right] - \frac{\partial}{\partial n_z}\int_S \frac{\partial}{\partial n}\left[\frac{1}{R}\left[g\right]_{t_R}\right] d\mathbf{x}_s \tag{15}$$

In equation (15), $\frac{\partial}{\partial n_z}$ is the normal derivative with respect to $\mathbf{z}$ at boundary point $\mathbf{z}_s$. By the boundary condition involving the exact Green's function,

$$\frac{\partial}{\partial n_z} g\left(\mathbf{z}_s, \mathbf{y}, t, s\right) = 0$$

equation (15) reduces to

$$4\pi \frac{\partial C_s}{\partial n_z} g(\mathbf{z}_s, \mathbf{y}, t, s) = \frac{\partial}{\partial n_z}\left[\frac{1}{r} q\left(t-s-r\right)\right] - \frac{\partial}{\partial n_z}\int_S \frac{\partial}{\partial n}\left[\frac{1}{R}\left[g\right]_{t_R}\right] d\mathbf{x}_s \tag{16}$$

A combination of (14) and (16) results in

$$\begin{aligned}(1-a)\, 4\pi C_s \frac{\partial g}{\partial t}\left(\mathbf{z}_s, \mathbf{y}, t, s\right) + ac4\pi \frac{\partial C_s}{\partial n_z} g(\mathbf{z}_s, \mathbf{y}, t, s) &= (1-a)\frac{1}{r}\frac{\partial q}{\partial t}\left(t-s-r\right) + ac\frac{\partial}{\partial n_z}\left[\frac{1}{r} q\left(t-s-r\right)\right] \\ -(1-a)\int_S \frac{\partial}{\partial n}\left[\frac{1}{R}\left[\frac{\partial g}{\partial t}\right]_{t_R}\right] d\mathbf{x}_s - ac\frac{\partial}{\partial n_z}\int_S \frac{\partial}{\partial n}\left[\frac{1}{R}\left[g\right]_{t_R}\right] d\mathbf{x}_s &\end{aligned} \tag{17}$$

where $a \in (0,1)$ is a coupling parameter and c is chosen so that all terms in the equation have comparable orders of magnitude.[10] The Burton-Miller formulation yields unique solutions for all frequencies.[12]

IV.B. Treatment of Hypersingular Integrals

The main difficulty in using any Burton-Miller formulation is dealing with hypersingular integrals that arise when taking the normal derivative of the original boundary integral equation. With arguments written explicitly, equation (17) is

$$\begin{aligned}(1-a)\, 4\pi C_s \frac{\partial g}{\partial t}\left(\mathbf{z}_s, \mathbf{y}, t, s\right) + ac4\pi \frac{\partial C_s}{\partial n_z} g(\mathbf{z}_s, \mathbf{y}, t, s) &= (1-a)\frac{1}{r}\frac{\partial q}{\partial t}\left(t-s-r\right) + ac\frac{\partial}{\partial n_z}\left[\frac{1}{r} q\left(t-s-r\right)\right] \\ -(1-a)\int_S \frac{\partial}{\partial n}\left[\frac{1}{R}\left[\frac{\partial g}{\partial t}\left(\mathbf{x}_s, \mathbf{y}, t-R, s\right)\right]\right] d\mathbf{x}_s - ac\frac{\partial}{\partial n_z}\int_S \frac{\partial}{\partial n}\left[\frac{1}{R}\left[g\left(\mathbf{x}_s, \mathbf{y}, t-R, s\right)\right]\right] d\mathbf{x}_s &\end{aligned} \tag{18}$$

Downloaded by Fang Hu on August 28, 2016 | http://arc.aiaa.org | DOI: 10.2514/6.2007-3479

In equation (18), the last term will involve a hypersingular integral because

$$\frac{\partial^2}{\partial n_z \partial n}\left[\frac{1}{R}\right] = O\left(\frac{1}{R^3}\right) \tag{19}$$

To reduce the singularity, the hypersingular integrals are regularized by an approach used by Liu et. al.[13] and Hwang[14] for the frequency-domain Burton-Miller formulation. Consider the relation for determining C_s[13]

$$4\pi C_s = 4\pi - \int_S \frac{\partial G_0}{\partial n} d\mathbf{x}_s \tag{20}$$

where $G_0 = \frac{1}{R}$. Multiplying both sides of equation (20) by $g(\mathbf{z}, \mathbf{y}, t, s)$ results in

$$4\pi C_s g(\mathbf{z}, \mathbf{y}, t, s) = 4\pi g(\mathbf{z}, \mathbf{y}, t, s) - \int_S \frac{\partial G_0}{\partial n} g(\mathbf{z}, \mathbf{y}, t, s)\, d\mathbf{x}_s$$

By taking the normal derivative with respect to $\mathbf{z}$ at the boundary, and using the boundary condition for g, the above becomes

$$4\pi \frac{\partial C_s}{\partial n_z} g(\mathbf{z}_s, \mathbf{y}, t, s) = -\frac{\partial}{\partial n_z} \int_S \frac{\partial G_0}{\partial n} g(\mathbf{z}_s, \mathbf{y}, t, s)\, d\mathbf{x}_s \tag{21}$$

Equation (21) is substituted into equation (18) to get

$$(1-a)\, 4\pi C_s \frac{\partial g}{\partial t}(\mathbf{z}_s, \mathbf{y}, t, s) - ac \frac{\partial}{\partial n_z} \int_S g(\mathbf{z}_s, \mathbf{y}, t, s) \frac{\partial G_0}{\partial n} d\mathbf{x}_s = (1-a)\frac{1}{r}\frac{\partial q}{\partial t}(t-s-r)$$

$$+ac \frac{\partial}{\partial n_z}\left[\frac{1}{r} q(t-s-r)\right] - (1-a)\int_S \frac{\partial}{\partial n}\left[G_0\left[\frac{\partial g}{\partial t}(\mathbf{x}_s, \mathbf{y}, t-R, s)\right]\right] d\mathbf{x}_s$$

$$-ac \frac{\partial}{\partial n_z}\int_S \frac{\partial}{\partial n}\left[G_0\left[g(\mathbf{x}_s, \mathbf{y}, t-R, s)\right]\right] d\mathbf{x}_s$$

Rearranging the terms, we get

$$(1-a)\, 4\pi C_s \frac{\partial g}{\partial t}(\mathbf{z}_s, \mathbf{y}, t, s) = (1-a)\frac{1}{r}\frac{\partial q}{\partial t}(t-s-r) + ac \frac{\partial}{\partial n_z}\left[\frac{1}{r} q(t-s-r)\right]$$

$$-(1-a)\int_S \frac{\partial G_0}{\partial n}\left[g(\mathbf{x}_s, \mathbf{y}, t-R, s) + R\frac{\partial g}{\partial t}(\mathbf{x}_s, \mathbf{y}, t-R, s)\right] d\mathbf{x}_s$$

$$-ac \frac{\partial}{\partial n_z}\int_S \frac{\partial G_0}{\partial n}\left[g(\mathbf{x}_s, \mathbf{y}, t-R, s) - g(\mathbf{z}_s, \mathbf{y}, t-R, s) + R\frac{\partial g}{\partial t}(\mathbf{x}_s, \mathbf{y}, t-R, s)\right] d\mathbf{x}_s \tag{22}$$

In particular, note that the last term in equation (22) is

$$\frac{\partial}{\partial n_z}\int_S \frac{\partial G_0}{\partial n}\left[g(\mathbf{x}_s, \mathbf{y}, t-R, s) - g(\mathbf{z}_s, \mathbf{y}, t, s) + R\frac{\partial g}{\partial t}(\mathbf{x}_s, \mathbf{y}, t-R, s)\right] d\mathbf{x}_s$$

$$= \int_S \frac{\partial^2 G_0}{\partial n_z \partial n}\left[g(\mathbf{x}_s, \mathbf{y}, t-R, s) - g(\mathbf{z}_s, \mathbf{y}, t, s) + R\frac{\partial g}{\partial t}(\mathbf{x}_s, \mathbf{y}, t-R, s)\right]$$

$$+\frac{\partial G_0}{\partial n}\left[\frac{\partial g}{\partial t}(\mathbf{x}_s, \mathbf{y}, t-R, s)\left(-\frac{\partial R}{\partial n_z}\right) + \frac{\partial}{\partial n_z}\left[R\frac{\partial g}{\partial t}(\mathbf{x}_s, \mathbf{y}, t-R, s)\right]\right] d\mathbf{x}_s$$

$$= \int_S \frac{\partial^2 G_0}{\partial n_z \partial n}\left[g(\mathbf{x}_s, \mathbf{y}, t-R, s) - g(\mathbf{z}_s, \mathbf{y}, t, s) + R\frac{\partial g}{\partial t}(\mathbf{x}_s, \mathbf{y}, t-R, s)\right] d\mathbf{x}_s$$

$$-\int_S R\frac{\partial G_0}{\partial n}\frac{\partial R}{\partial n_z}\frac{\partial^2 g}{\partial t^2}(\mathbf{x}_s, \mathbf{y}, t-R, s)\, d\mathbf{x}_s \tag{23}$$

Note that the first integrand in equation (23) becomes (Appendix)

$$\frac{\partial^2 G_0}{\partial n_z \partial n}\left[g(\mathbf{x}_s, \mathbf{y}, t-R, s) - g(\mathbf{z}_s, \mathbf{y}, t, s) + R\frac{\partial g}{\partial t}(\mathbf{x}_s, \mathbf{y}, t-R, s)\right]$$

Downloaded by Fang Hu on August 28, 2016 | http://arc.aiaa.org | DOI: 10.2514/6.2007-3479

$$= \frac{\partial^2 G_0}{\partial n_z \partial n} \nabla g\left(\mathbf{z}_s, \mathbf{y}, t, s\right) \cdot \mathbf{R}$$

which renders the above integrable with a principal value. Thus, the regularized integral equation is

$$(1-a)\,4\pi C_s \frac{\partial g}{\partial t}\left(\mathbf{z}_s, \mathbf{y}, t, s\right) = (1-a)\,\frac{1}{r}\frac{\partial q}{\partial t}\left(t-s-r\right) + ac\frac{\partial}{\partial n_z}\left[\frac{1}{r}q\left(t-s-r\right)\right]$$

$$-(1-a)\int_S \frac{\partial}{\partial n}\left[G_0\left[\frac{\partial g}{\partial t}\left(\mathbf{x}_s, \mathbf{y}, t-R, s\right)\right]\right] d\mathbf{x}_s - ac\int_S \frac{\partial^2 G_0}{\partial n_z \partial n}\left[g\left(\mathbf{x}_s, \mathbf{y}, t-R, s\right)\right.$$

$$\left.-g\left(\mathbf{z}_s, \mathbf{y}, t, s\right) + R\frac{\partial g}{\partial t}\left(\mathbf{x}_s, \mathbf{y}, t-R, s\right)\right] d\mathbf{x}_s - ac\int_S R\frac{\partial G_0}{\partial n}\frac{\partial R}{\partial n_z}\frac{\partial^2 g}{\partial t^2}\left(\mathbf{x}_s, \mathbf{y}, t-R, s\right) d\mathbf{x}_s \tag{24}$$

or

$$(1-a)\,4\pi C_s \frac{\partial g}{\partial t}\left(\mathbf{z}_s, \mathbf{y}, t, s\right) = (1-a)\,\frac{1}{r}\frac{\partial q}{\partial t}\left(t-s-r\right) + ac\frac{\partial}{\partial n_z}\left[\frac{1}{r}q\left(t-s-r\right)\right]$$

$$-(1-a)\int_S \frac{\partial G_0}{\partial n}\frac{\partial g}{\partial t}\left(\mathbf{x}_s, \mathbf{y}, t-R, s\right) + R\frac{\partial G_0}{\partial n}\frac{\partial^2 g}{\partial t^2}\left(\mathbf{x}_s, \mathbf{y}, t-R, s\right) d\mathbf{x}_s$$

$$-ac\int_S \frac{\partial^2 G_0}{\partial n_z \partial n}\left[g\left(\mathbf{x}_s, \mathbf{y}, t-R, s\right) - g\left(\mathbf{z}_s, \mathbf{y}, t, s\right) + R\frac{\partial g}{\partial t}\left(\mathbf{x}_s, \mathbf{y}, t-R, s\right)\right] d\mathbf{x}_s$$

$$-ac\int_S R\frac{\partial G_0}{\partial n}\frac{\partial R}{\partial n_z}\frac{\partial^2 g}{\partial t^2}\left(\mathbf{x}_s, \mathbf{y}, t-R, s\right) d\mathbf{x}_s \tag{25}$$

At collocation point $\mathbf{z}_k$ and time step t_j, equation (25) becomes

$$(1-a)\,4\pi C_s \sum_{n=0}^{N_t}\sum_{i=1}^{N} u_i^n \phi_i(\mathbf{z}_k)\psi_n'(t_j) = (1-a)\,\frac{1}{r}\frac{\partial q}{\partial t}\left(t_j-s-r\right) + ac\frac{\partial}{\partial n_z}\left[\frac{1}{r}q\left(t_j-s-r\right)\right]$$

$$-(1-a)\int_S \frac{\partial G_0}{\partial n}\sum_{n=0}^{N_t}\sum_{i=1}^{N} u_i^n \phi_i(\mathbf{x}_s)\psi_n'(t_j-R) + R\frac{\partial G_0}{\partial n}\sum_{n=0}^{N_t}\sum_{i=1}^{N} u_i^n \phi_i(\mathbf{x}_s)\psi_n''(t_j-R)d\mathbf{x}_s$$

$$-ac\int_S \frac{\partial^2 G_0}{\partial n_z \partial n}\left[\sum_{n=0}^{N_t}\sum_{i=1}^{N} u_i^n \phi_i(\mathbf{x}_s)\psi_n(t_j-R) - \sum_{n=0}^{N_t}\sum_{i=1}^{N} u_i^n \phi_i(\mathbf{z}_k)\psi_n(t_j) + R\sum_{n=0}^{N_t}\sum_{i=1}^{N} u_i^n \phi_i(\mathbf{x}_s)\psi_n'(t_j-R)\right] d\mathbf{x}_s$$

$$+ac\int_S R\frac{\partial G_0}{\partial n}\frac{\partial R}{\partial n_z}\sum_{n=0}^{N_t}\sum_{i=1}^{N} u_i^n \phi_i(\mathbf{x}_s)\psi_n''(t_j-R)d\mathbf{x}_s \tag{26}$$

Equation (26) can again be written as a time marching scheme, i.e.,

$$\mathbf{B}_0\mathbf{u}^j = \mathbf{q}^j - \sum_{m=1}^{j}\mathbf{B}_m\mathbf{u}^{j-m}$$

which results in

$$\{\mathbf{B}_m\}_{ki} = (1-a)\,4\pi C_s \phi_i(\mathbf{z}_k)\psi_{j-m}'(t_j) + (1-a)\int_S \frac{\partial G_0}{\partial n}\phi_i(\mathbf{x}_s)\psi_{j-m}'(t_j-R)d\mathbf{x}_s$$

$$+(1-a)\int_S R\frac{\partial G_0}{\partial n}\phi_i(\mathbf{x}_s)\psi_{j-m}''(t_j-R)d\mathbf{x}_s + ac\int_S \frac{\partial^2 G_0}{\partial n_z \partial n}\left[\phi_i(\mathbf{x}_s)\psi_{j-m}(t_j-R)\right.$$

$$\left.-\phi_i(\mathbf{z}_k)\psi_{j-m}(t_j) + R\phi_i(\mathbf{x}_s)\psi_{j-m}'(t_j-R)\right] d\mathbf{x}_s - ac\int_S R\frac{\partial G_0}{\partial n}\frac{\partial R}{\partial n_z}\phi_i(\mathbf{x}_s)\psi_{j-m}''(t_j-R)d\mathbf{x}_s \tag{27}$$

Note that since $\phi_i(\mathbf{x}_s)$ is non-zero only when $\mathbf{x}_s \in S_i$, the terms belonging to the matrix $\mathbf{B}_m$ are

$$\{\mathbf{B}_m\}_{ki} = (1-a)\,4\pi C_s \phi_i\left(\mathbf{z}_k\right)\psi_{j-m}'\left(t_j\right) + (1-a)\int_{S_i}\frac{\partial G_0}{\partial n}\phi_i\left(\mathbf{x}_s\right)\psi_{j-m}'\left(t_j-R\right)d\mathbf{x}_s$$

Downloaded by Fang Hu on August 28, 2016 | http://arc.aiaa.org | DOI: 10.2514/6.2007-3479

$$+(1-a)\int_{S_i} R\frac{\partial G_0}{\partial n}\phi_i(\mathbf{x}_s)\,\psi''_{j-m}(t_j-R)\,d\mathbf{x}_s + ac\int_{S_i}\frac{\partial^2 G_0}{\partial n_z \partial n}\left[\phi_i(\mathbf{x}_s)\,\psi_{j-m}(t_j-R) - \phi_i(\mathbf{z}_k)\,\psi_{j-m}(t_j)\right.$$

$$\left.+R\phi_i(\mathbf{x}_s)\,\psi'_{j-m}(t_j-R)\right]d\mathbf{x}_s - ac\int_{S_i} R\frac{\partial G_0}{\partial n}\frac{\partial R}{\partial n_z}\phi_i(\mathbf{x}_s)\,\psi''_{j-m}(t_j-R)\,d\mathbf{x}_s$$

$$-ac\int_{S-S_i}\frac{\partial^2 G_0}{\partial n_z \partial n}\phi_i(\mathbf{z}_k)\,\psi_{j-m}(t_j)\,d\mathbf{x}_s \tag{28}$$

As in the original time-domain formulation, the matrix $\mathbf{B}_0$ is a sparse matrix.

V. Results of Time-domain BEM using Burton-Miller Formulation

Consider a sphere of radius 0.5 with a boundary consisting of $N = 760$ curved triangular elements. Figure 6 and Figure 7 represent the results obtained when the time-domain BEM is revised using the modified Burton-Miller formulation for $\omega_0 = 6\pi$ and $\omega_0 = 4\pi$ respectively. For comparison purposes, the expansion coefficient plotted corresponds to the node located at $\mathbf{z}_s = (0.0514, 0.00814, 0.497)$, the basis function order is $P = 0$, the source point is at $\mathbf{y} = (0, 0, 10)$ and the time step size is $\Delta t = 0.05$. All calculations involving the Burton-Miller formulation were performed with $c = -1$. Compared with Figure 4 and Figure 5, Figure

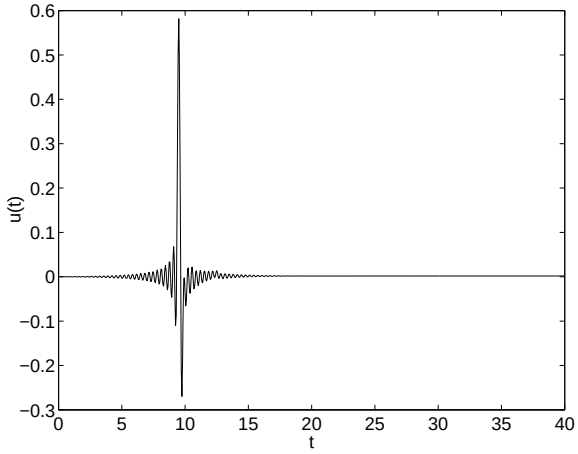

Figure 6. Transient numerical solution $u(t)$ at $\mathbf{z}_s = (0.0514, 0.00814, 0.497)$ using Burton-Miller Formulation. The source function frequency is $\omega_0 = 6\pi$ and the coupling parameter is $a = 0.5$.

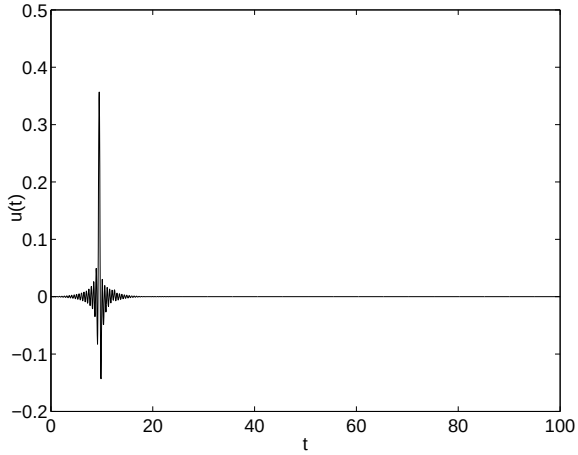

Figure 7. Transient numerical solution $u(t)$ at $\mathbf{z}_s = (0.0514, 0.00814, 0.497)$ using Burton-Miller Formulation. The source function frequency is $\omega_0 = 4\pi$ and the coupling parameter is $a = 0.5$.

6 and Figure 7 show the effectiveness of the Burton-Miller formulation in dealing with long-time instabilities that arise in many March-On-Time schemes.

Downloaded by Fang Hu on August 28, 2016 | http://arc.aiaa.org | DOI: 10.2514/6.2007-3479

To demonstrate the accuracy of the time-domain Boundary Element Method with a modified Burton-Miller Combined Field Integral Equation, consider again the sphere of radius 0.5 with 760 curved triangular boundary elements. Let the source point be located at $\mathbf{y} = (0, 0, 10)$ and let the spatial basis function order be $P = 0$. A Fourier transform of $u(t)$ gives the solution at all frequencies. In this case, the exact solution in the frequency domain for $M = 0$ is well-known and therefore it is utilized in this section as the basis of comparison. Figure 8 shows comparisons with the exact solution for $\omega = 2\pi$ and $\omega = 4\pi$ with source function frequency $\omega_0 = 4\pi$, $a = 0.5$, $c = -1$ and $h = 0.2\pi$.

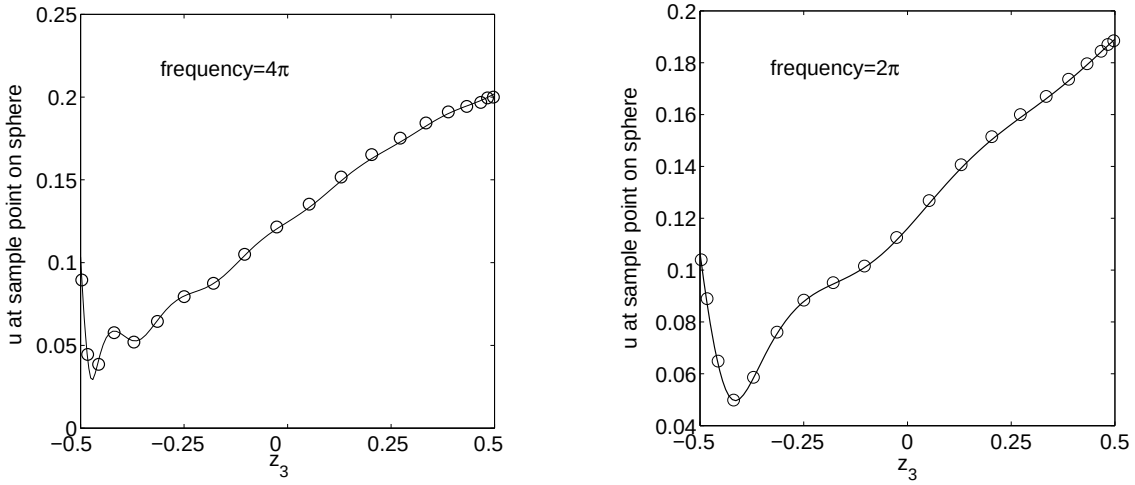

Figure 8. Comparison with exact solution (solid line) at selected frequencies.

V.A. Effects of Changing Parameter c

Until now, the parameter affecting the relative magnitudes of the time derivative and normal derivative parts of the Burton-Miller boundary integral equation has been set at $c = -1$. Figure 9 illustrates the effects of changing c for frequency $\omega = 2\pi$. Again, the exact solution in the frequency domain is used as the basis of comparison. The results in Figure 9 are for source function frequency $\omega_0 = 2\pi$, $a = 0.5$, $h = 0.2\pi$ and $\Delta t = 0.05$. Figure 9 demonstrates that the choice of the parameter c does not have a large effect on the accuracy of the results.

V.B. Effects of Changing Δt

As stated previously in section *II.C.1*, if the time step is chosen so that $\Delta t < R_{min}$ where R_{min} is the minimum distance between collocation point and quadrature points, then the matrix $\mathbf{B}_0$ in the March-On-Time scheme will be a diagonal matrix. For the case of the spherical boundary of radius 0.5 with 760 curved triangular elements, the maximum time step value that will make $\mathbf{B}_0$ diagonal is $\Delta t \approx 0.0096$. A diagonal matrix $\mathbf{B}_0$ causes a significant decrease in computation time over a non-diagonal $\mathbf{B}_0$, and so the diagonal matrix is preferred. This section contains a study of the effects of changing Δt on the accuracy of the numerical Burton-Miller results when compared with exact solutions.

All results in this section correspond to a source point location of $\mathbf{y} = (0, 0, 10)$ and a spatial basis function order of $P = 0$. Other terms kept constant are $a = 0.5$, $c = -1$ and $h = 0.2\pi$. Figure 10 is a plot of the numerical results versus the exact solution for frequency $\omega = 2\pi$ and source function frequency $\omega_0 = 4\pi$ at several time step values. Figure 11 shows similar results for frequency $\omega = 4\pi$, also with source function frequency $\omega_0 = 4\pi$. For frequency $\omega = 2\pi$, decreasing Δt does not improve the accuracy of the numerical results. However, for frequency $\omega = 4\pi$, $\Delta t = 0.025$ and $\Delta t = 0.01$ result in improvements in accuracy over $\Delta t = 0.05$. Both figures illustrate the effects of Δt on the accuracy of the results. As Δt decreases, the numerical results will become more accurate until a minimum value is reached. This minimum value of Δt varies with frequency.

Downloaded by Fang Hu on August 28, 2016 | http://arc.aiaa.org | DOI: 10.2514/6.2007-3479

Downloaded by Fang Hu on August 28, 2016 | http://arc.aiaa.org | DOI: 10.2514/6.2007-3479

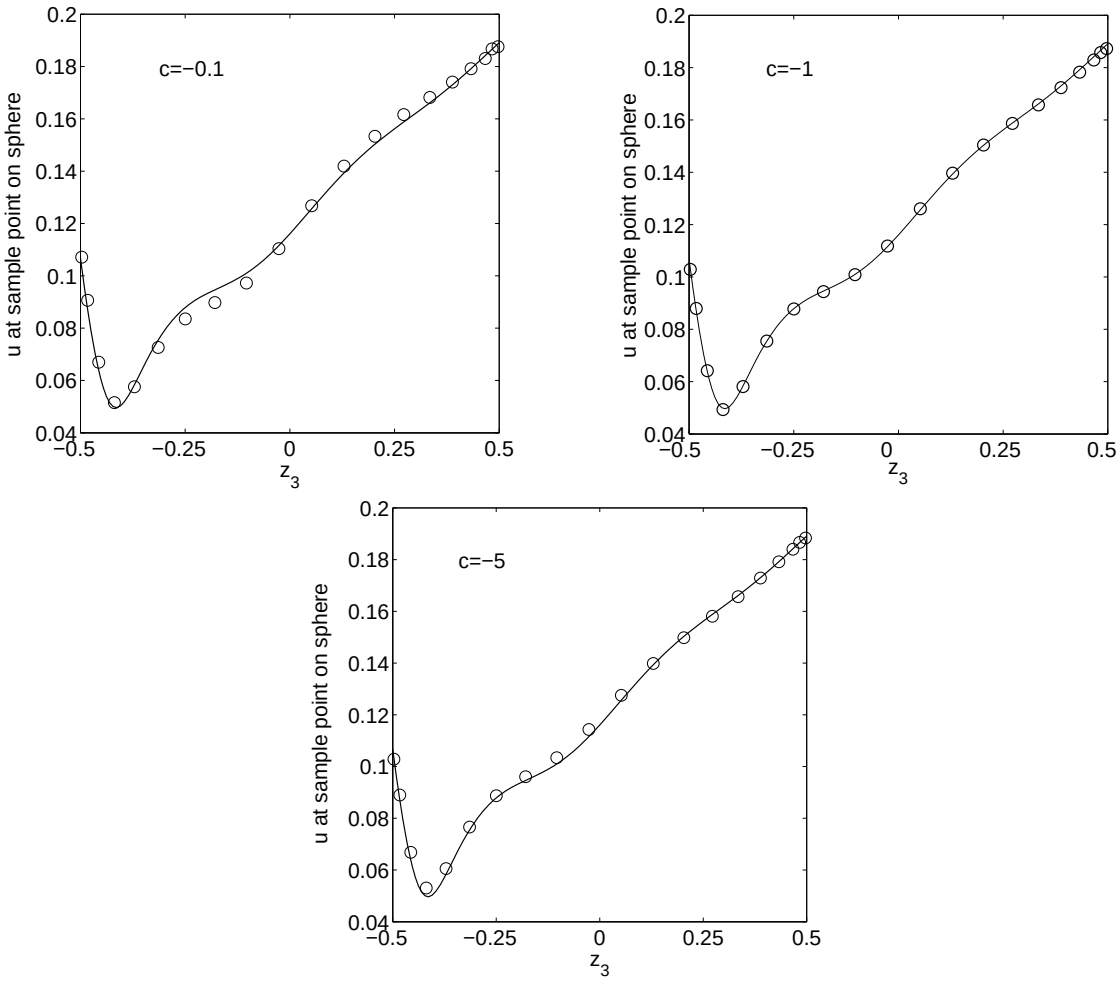

Figure 9. Comparison with exact solution (solid line) for $\omega = 2\pi$ and selected values of c.

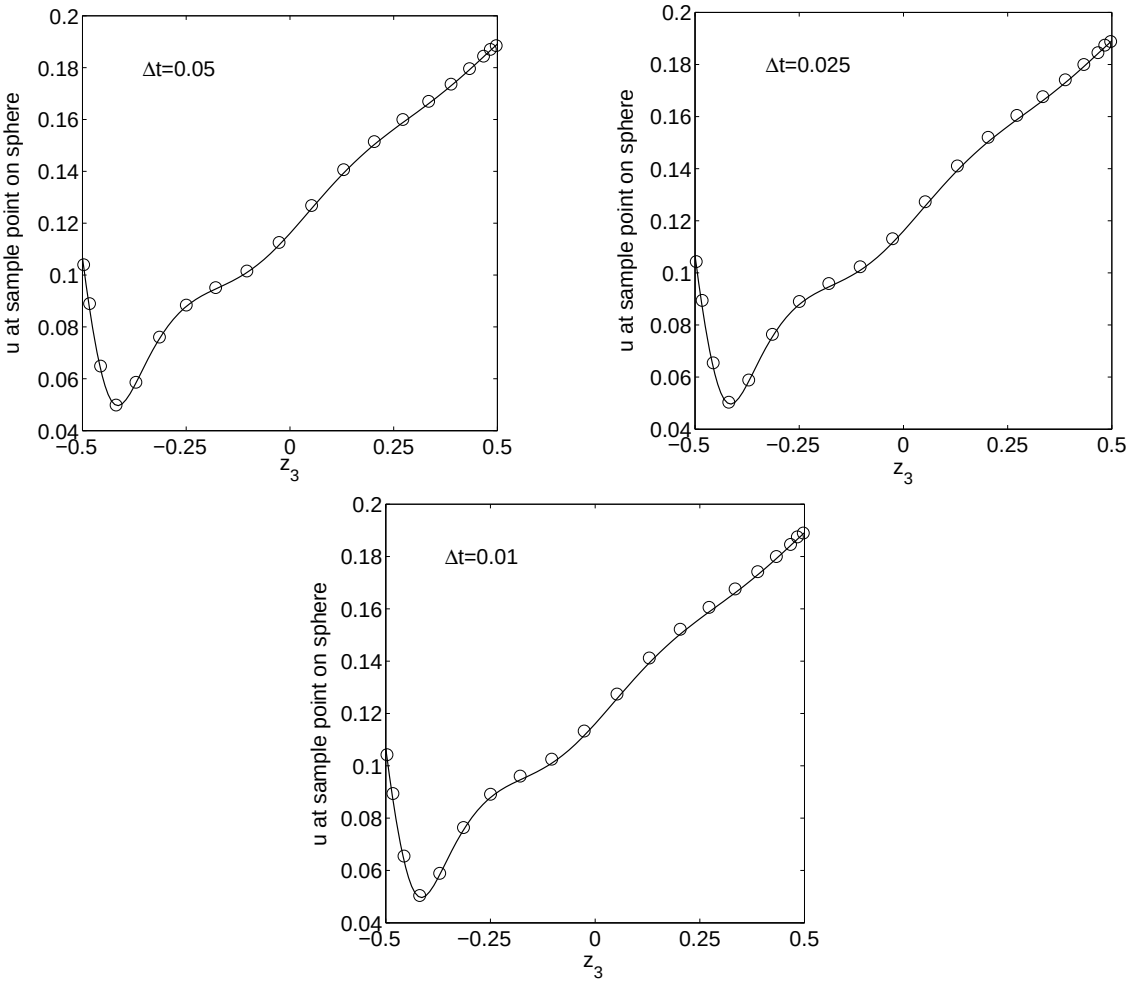

Figure 10. Comparison with exact solution (solid line) for $\omega = 2\pi$ and selected values of Δt.

Downloaded by Fang Hu on August 28, 2016 | http://arc.aiaa.org | DOI: 10.2514/6.2007-3479

V.C. Effects of Source Function Shape

In a final study, consider again the sphere of radius 0.5 with $N = 760$ curved triangular elements. Let $\mathbf{y} = (0, 0, 10)$, $P = 0$, $a = 0.5$, $c = -1$ and $\Delta t = 0.025$. As stated previously, the source function, $q(t)$, has a spectrum of unity over the frequency range of interest. The parameter h determines the shape of the source function and can be adjusted as the source function frequency, ω_0, changes in order to maintain a spectrum of unity over the desired frequency range.

Figure 12 compares the numerical Burton-Miller results with the exact solution for several points located on the sphere's boundary. The graph on the right in Figure 12 shows a loss of accuracy for many of the boundary points when $\omega_0 = 2\pi$ with $h = 1.2\pi$. In order to ensure an accurate solution, the source function frequency ω_0 should be greater than or equal to the desired solution frequency ω.

VI. Conclusions

A three-dimensional time-domain Boundary Element Method has been presented for computing exact Green's functions in acoustic analogy. A March-On-Time scheme was formulated to solve the time-domain boundary integral equation. Numerical examples showed the long-time instabilities associated with the time-marching scheme. Using a modified Burton-Miller Combined Field Integral Equation, long-time instability problems were corrected. Hypersingular integrals arising from the Burton-Miller formulation were regularized by a normal derivative of the boundary integral constant. Examples of the time-domain Boundary Element Method with the Burton-Miller modification compared numerical results to the exact solution for a sphere

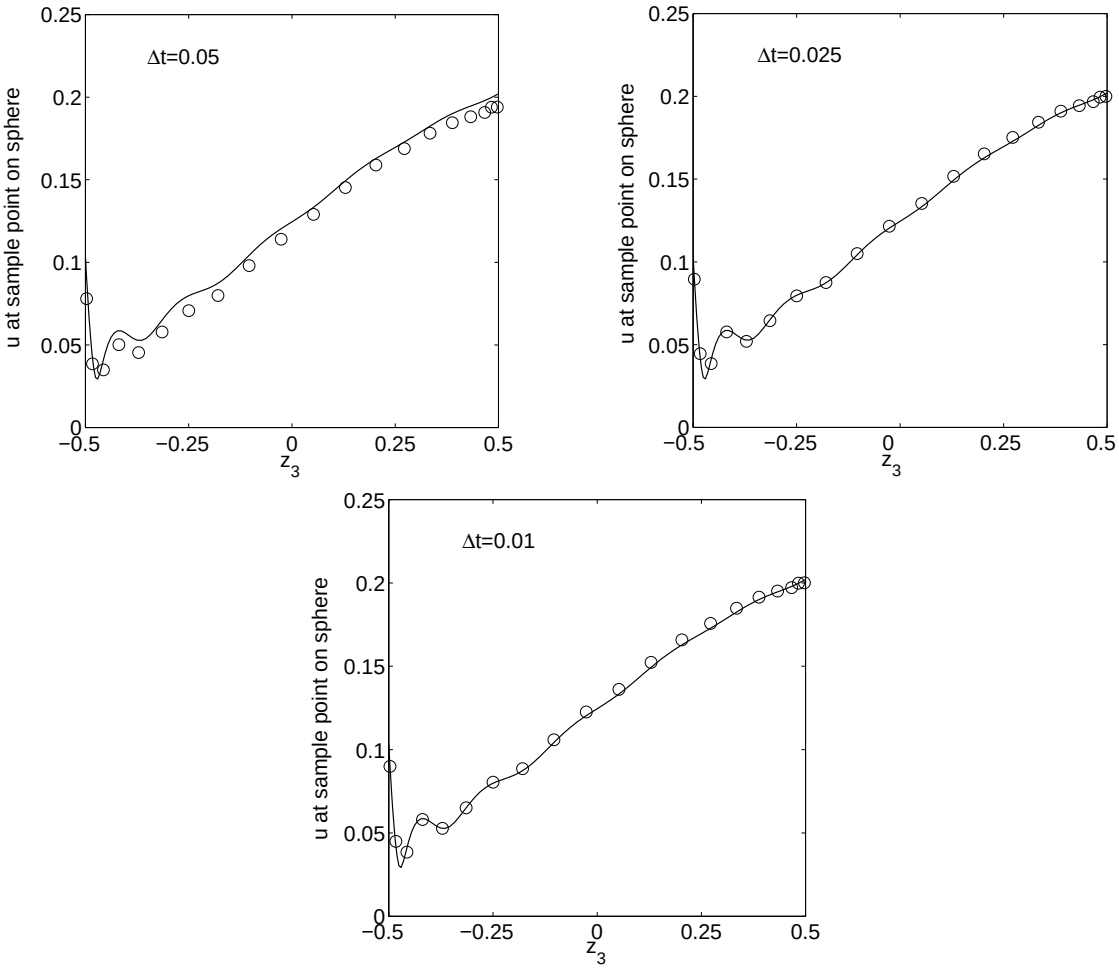

Figure 11. Comparison with exact solution (solid line) for $\omega = 4\pi$ and selected values of Δt.

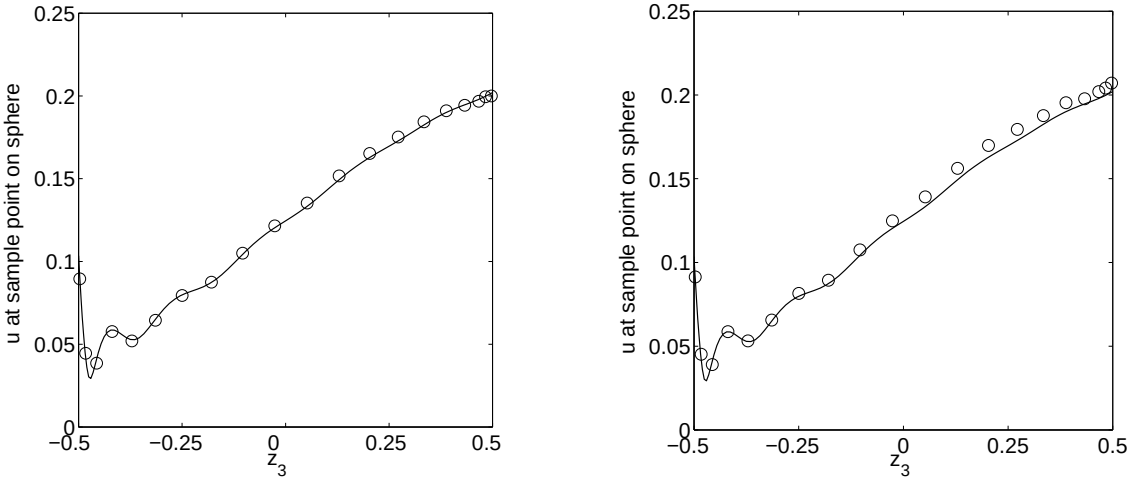

Figure 12. Comparison with exact solution (solid line) for $\omega = 4\pi$. The source function frequency is $\omega_0 = 4\pi$ with $h = 0.2\pi$ (left) and $\omega_0 = 2\pi$ with $h = 1.2\pi$ (right).

Downloaded by Fang Hu on August 28, 2016 | http://arc.aiaa.org | DOI: 10.2514/6.2007-3479

with good agreement. The effects of changing the parameters c and h were discussed. No significant improvement in accuracy resulted from changes in c. In the last example, the results worsened for higher values of h. Therefore, ω_0 should be at least as large as ω. The effects of changing Δt were also studied. For each frequency, a decrease in Δt causes improvements in numerical solution accuracy until a minimum value is reached. As a result, the matrix $\mathbf{B}_0$ can be formulated as a diagonal matrix without loss of accuracy. With the correct choice of Δt, the modified Burton-Miller scheme gives both accurate and stable results.

Appendix

The regularized integrand for the hypersingular integral, given in section IV.B, has the form of

$$\frac{\partial^2 G_0}{\partial n_z \partial n}[g(\mathbf{x}_s, \mathbf{y}, t-R, s) - g(\mathbf{z}, \mathbf{y}, t, s) + R\frac{\partial g}{\partial t}(\mathbf{x}_s, \mathbf{y}, t-R, s)]$$

$$= \frac{\partial^2 G_0}{\partial n_z \partial n}[\nabla g(\mathbf{z}, \mathbf{y}, t, s) \cdot \mathbf{R} + O(R^2)] \tag{29}$$

Therefore, if constant element spatial basis function is used, i.e., $P = 0$, we have $\nabla g \equiv 0$ and (29) is integrable in the regular sense. When linear or higher-order spatial basis functions are used, (29) becomes integrable using the Cauchy principal value.[12]

Recalling the element parametrization form given in equation (19), we can evaluate the integral for (29) by the polar coordinates centered at the nodal point $\mathbf{x}_k$. Denote its integrand by $F(r, \theta)$ as

$$F(r,\theta) = \frac{\partial^2 G_0}{\partial n_z \partial n}[g(\mathbf{x}_s, \mathbf{y}, t-R, s) - g(\mathbf{z}, \mathbf{y}, t, s) + R\frac{\partial g}{\partial t}(\mathbf{x}_s, \mathbf{y}, t-R, s)]|\mathbf{x}_\xi \times \mathbf{x}_\eta| \tag{30}$$

and the limit

$$\lim_{r\to 0} r^2 F(r,\theta) = \bar{G}(\theta)$$

where it has been found that

$$\bar{G}(\theta) = \frac{(\mathbf{n}_z \cdot \mathbf{n}_s)\nabla g(\mathbf{x}_k, \mathbf{y}, t, s) \cdot [(\mathbf{b} + 2\xi_k \mathbf{d} + \eta_k \mathbf{f})\cos\theta + (\mathbf{c} + \xi_k \mathbf{f} + 2\eta_k \mathbf{e})\sin\theta]}{|[(\mathbf{b} + 2\xi_k \mathbf{d} + \eta_k \mathbf{f})\cos\theta + (\mathbf{c} + \xi_k \mathbf{f} + 2\eta_k \mathbf{e})\sin\theta]|^3}|\mathbf{x}_\xi \times \mathbf{x}_\eta|_{r=0} \tag{31}$$

Then, the integral on a hypersingular element S_k can be evaluated as follows,

$$\int_{S_k} F(r,\theta)dS = \lim_{\epsilon\to 0}\int_0^{2\pi}\int_\epsilon^{r(\theta)} F(r,\theta) r dr d\theta$$

$$= \lim_{\epsilon\to 0}\int_0^{2\pi}\int_\epsilon^{r(\theta)} [\frac{r^2 F(r,\theta) - \bar{G}(0,\theta)}{r} + \frac{\bar{G}(0,\theta)}{r}] dr d\theta$$

$$= \int_0^{2\pi}\int_0^{r(\theta)} \frac{r^2 F(r,\theta) - \bar{G}(0,\theta)}{r} dr d\theta + \lim_{\epsilon\to 0}\int_0^{2\pi} \bar{G}(0,\theta)[\ln r(\theta) - \ln\epsilon] d\theta$$

$$= \int_0^{2\pi}\int_0^{r(\theta)} \frac{r^2 F(r,\theta) - \bar{G}(0,\theta)}{r} dr d\theta + \int_0^{2\pi} \bar{G}(0,\theta)\ln r(\theta) d\theta$$

where it is easy to verify that

$$\int_0^{2\pi} \bar{G}(0,\theta) d\theta = 0$$

Downloaded by Fang Hu on August 28, 2016 | http://arc.aiaa.org | DOI: 10.2514/6.2007-3479

Acknowledgments

This work is supported by a grant from the NASA Langley Research Center, NAG1-03037. The technical monitor is Dr. Mehdi R. Khorrami. This work is also supported by an Old Dominion University College of Sciences Dissertation Fellowship.

References

[1]Y. P. Guo, "Airframe Noise Prediction by Acoustic Analogy", NASA Report NAS1-00086, 2004.

[2]F. Q. Hu, Y. P. Guo and A. D. Jones, "On computation and application of exact Green's function in acoustic analogy", AIAA paper 2005-2985, 2005.

[3]A. D. Jones and F. Q. Hu, "An investigation of spectral collocation boundary element method for the computation of exact Green's function in acoustic analogy", AIAA paper 2005-2636, 2006.

[4]A. A. Ergin, B. Shanker and E. Michielssen, "Analysis of transient wave scattering from rigid bodies using a Burton-Miller approach", Journal of Acoustical Society of America, Vol. 106, No. 5, 2396-2404, 1999.

[5]A. A. Ergin, B. Shanker and E. Michielssen, "Fast analysis of transient acoustic wave scattering from rigid bodies using the multilevel plane wave time domain algorithm", Journal of Acoustical Society of America, Vol. 107, No. 3, 1168-1178, 2000.

[6]G. Strang and G. Fix, *An analysis of the finite element method*, Prentice-Hall, 1973.

[7]M. G. Blyth and A. Pozrikidis, "A Lobatto interpolation grid over the triangle", IMA Journal of Applied Mathematics, Vol. 71, 153-169, 2006.

[8]C. Pozrikidis, *A practical guide to boundary element methods with the software library BEMLIB*, Chapman & Hall/CRC, 2002.

[9]C. Pozrikidis, "A spectral collocation method with triangular boundary elements", Engrg. Anal. Bound. Elem., Vol. 30, 315-324, 2006.

[10]D. J. Chappell, P. J. Harris, D. Henwood, R. Chakrabarti, "A stable boundary element method for modeling transient acoustic radiation", Journal of Acoustical Society of America, Vol. 120, No. 1, 74-80, 2006.

[11]A. J. Burton, G. F. Miller, "The application of integral equation methods to the numerical solution of some exterior boundary-value problems", Proc. Roy. Soc. Lond. A., Vol. 323, 201-210, 1971.

[12]T. W. Wu, A. F. Seybert, G. C. Wan, "On the numerical implementation of a Cauchy principal value integral to insure a unique solution for acoustic radiation and scattering", Journal of Acoustical Society of America, Vol. 90, No. 1, 554-560, 1991.

[13]G. R. Liu, C. Cai, J. Zhao, H. Zheng, K. Y. Lam, "A study on avoiding hyper-singular integrals in exterior acoustic radiation analysis", Applied Acoustics, Vol. 63, 643-657, 2002.

[14]W. S. Hwang, "Hypersingular boundary integral equations for exterior acoustic problems", Journal of Acoustical Society of America, Vol. 101, No. 6, 3336-3342, 1997.

Downloaded by Fang Hu on August 28, 2016 | http://arc.aiaa.org | DOI: 10.2514/6.2007-3479